An FDTD Model for Low and High Altitude Lightning-Generated EM Fields

Wenyi Hu and Steven A. Cummer, *Senior Member, IEEE*

***Abstract*—To explore lightning-generated electromagnetic wave behavior and lightning-related ionospheric phenomena, a full-wave two-dimensional cylindrical finite-difference time-domain (FDTD) model was developed to simulate lightning-generated electromagnetic wave propagation in the ionosphere with high altitude and long distance capabilities. This FDTD model removes the approximations made in other similar models to extend its applicability, and incorporates a variety of existing methods and new techniques. A dispersive and anisotropic realization of the nearly perfectly matched layer (NPML) absorbing boundary condition is adopted in this numerical model for ease of implementation. Earth curvature is included in the model through the modified refractive index method. The surface impedance boundary condition is adopted to treat arbitrary but homogeneous ground parameters. We quantify the errors through dispersion relations, and the solution convergence is analyzed. Comparisons between our simulation, numerical waveguide mode theory, and experimental data validate this model and show its capabilities compared to other methods. Although this FDTD model was developed for the lightning-generated electromagnetic field simulation, it is also applicable for other very low frequency (VLF, 3–30 kHz) and extremely low frequency (ELF, 3–3000 Hz) wave propagation problems.**

***Index Terms*—Electromagnetic propagation in plasma media, finite-difference time-domain (FDTD) methods, ionosphere, lightning.**

I. Introduction

LIGHTNING discharge currents are the most common natural sources in the Earth-ionosphere circuit. The very low frequency (VLF, 3–30 kHz) and extremely low frequency (ELF, 3–3000 Hz) electromagnetic waves radiated by these lightning currents propagate between the ground and ionosphere with low attenuation rates. The long-range detectability of these signals enables applications such as ionospheric remote sensing [1], [2] and remote lightning discharge current waveform measurement [3], [4]. The electromagnetic fields produced by intense lightning also modify the atmosphere, ionosphere and magnetosphere through a variety of processes. For example, high altitude (40–90 km) optical emissions above thunderstorms called sprites [5] are believed to be driven by the transient electric field in the mesosphere produced by intense lightning discharges [6], [7]. Although several theories were proposed in the past decade to explain various lightning-related ionospheric phenomena [6], [8], [9], some aspects of the phenomena still remain mysterious and detailed simulations can help understand the role of these processes. Additionally, VLF propagation in the Earth-ionosphere was commonly applied to long-distance communication and navigation before the era of GPS and satellite communication. Even today, submarine communication is still dependent on man-made VLF transmitters. These scientific and engineering applications require an accurate numerical model of lightning-generated electromagnetic fields for data analysis and theoretical predictions.

The most common mathematical formulations for the calculation of electromagnetic waves radiated by lightning discharges are based on the waveguide mode theory [10]–[12]. In mode theory, the atmosphere is treated as a dielectric layer between the reflecting boundaries, the ground and ionosphere. The fields in this waveguide can be expressed as the sum of the fields in independently propagating waveguide modes whose propagation properties (phase velocity, attenuation rate, and field structure) are a function of the boundaries. A mode theory formulation is especially efficient for long distances from the source because the variable attenuation rates ensure that only a small number of modes contribute significantly to the fields. Although it is inherently a frequency domain formulation, wide band time domain problems can be solved with an inverse Fourier transform. The mode theory solutions used in this work were calculated using the long wave propagation capability (LWPC) code [13] that is based on a complete two-dimensional (2-D) waveguide propagation formulation and can handle arbitrarily complex vertical inhomogeneities in the ionosphere.

An alternative approach is the finite-difference time domain method (FDTD) [14], which has some advantages over the mode theory. Arbitrarily complex inhomogeneities can be easily included in an FDTD calculation, while the horizontal inhomogeneities that mode theory can easily handle are limited [15]. Extending fields and sources to arbitrarily high altitudes in an FDTD code is also straightforward, but it is challenging to compute fields or include sources significantly above the main reflecting altitude ($\sim$80–90 km) using a numerical mode theory code.

FDTD has been used previously to model similar problems. Cho and Rycroft [16] developed a 2-D cylindrical model that includes electron heating caused by the quasielectrostatic field or the electromagnetic pulse to study the electrical breakdown in the mesosphere. They treated the ionospheric plasma as a simple isotropic conductor at all altitudes. The approximation of the plasma as a simple conductor is not valid above $\sim$90 km where the collision frequency is no longer much higher than the wave

Manuscript received June 2, 2005; revised November 16, 2005. This work was supported by NASA Geospace Sciences Grant NAG5-10270.

W. Hu was with the Department of Electrical and Computer Engineering, Duke University, Durham, NC 27708 USA. He is now with Schlumberger-Doll Research, Ridgefield, CT 06877 USA.

S. A. Cummer is with the Department of Electrical and Computer Engineering, Duke University, Durham, NC 27708 USA.

Digital Object Identifier 10.1109/TAP.2006.874336

frequency. Moreover, the anisotropy of the ionosphere due to Earth's magnetic field becomes significant above ∼60 km. The 2-D cylindrical model of Pasko *et al.* [17] with similar approximations was used to investigate the mechanism of the ELF radiation from sprites. Their model solves the full set of Maxwell equations but treats the ionosphere as a simple, isotropic conductor. Another 2-D cylindrical model developed by Veronis *et al.* [18] takes into account the nonlinear effects of heating and ionization. However, they also treated the ionosphere as a simple, isotropic conductor and no absorbing boundary condition (ABC) was used in their model, which makes it only applicable to low altitude (below 100 km) and small region simulations. Cummer [20] reported a 2-D cylindrical FDTD model that includes the anisotropy of the ionosphere but still assumes that the collision frequency is much higher than the wave frequency at all altitudes. Thèvenot *et al.* [21] developed another FDTD model for the computation of VLF-LF propagation in the ionosphere. Their 2-D spherical geometry model includes the background magnetic field but is only applicable to a single frequency source. Ma *et al.* [19] developed a three-dimensional (3-D) FDTD model to simulate the electrodynamic response of the atmosphere and ionosphere to the lightning discharges. Their model includes the anisotropic property of the ionosphere, but it still makes the simple conductor approximation and thus is limited to low altitudes and low frequencies. There are some other 3-D models [22]–[24] recently reported for Schumann resonance research. However, these 3-D models are only accurate to frequencies below several hundred Hz and they treat the ionosphere as a simple conductor. These models are thus not applicable to the higher frequency and higher altitude fields we simulate with this model.

The full wave electromagnetic 2-D cylindrical FDTD model we describe here removes those assumptions mentioned above and treats the ionosphere as a true cold plasma. This numerical model includes the effects of various charged particles (electrons, positive ions and negative ions). The nearly perfectly matched layer (NPML), a versatile ABC [25] that is simple to implement in the complicated linear medium needed here, was adopted. In concern of the complexity of this problem, we derive the coefficients of the iteration equations of FDTD numerically, which is more efficient in coding in comparison with the traditional analytical method. The surface impedance boundary condition (SIBC) [26], [27] is adopted to approximate the wave behaviors at the lossy ground. To accurately simulate high frequency fields and long-distance propagation, Earth curvature correction is included in this model. Compared with the previous FDTD models, this model extends the simulation altitude limitation from ∼100 km to ∼200 km and broadens the frequency range to ∼30 kHz. In addition, this model is more flexible in some aspects compared with the previous numerical models. We can easily specify the source geometry and use arbitrary source waveforms; the ground can be treated as PEC or arbitrary but homogeneous parameters; errors introduced by Earth curvature can be compensated without any extra computational cost; and spatial inhomogeneities and even nonlinear processes of the ionosphere can be easily included to solve more realistic problems without changing the main part of the code. In the following sections, we discuss the methods and techniques we used in this model in detail. Also, accuracy analysis is presented. The simulation results are compared with the mode theory solutions and broadband experimental data to validate this FDTD model. By simulating the fields in a large volume of space, this model is a powerful tool for calculating VLF and lower frequency electromagnetic fields produced by natural and controlled sources.

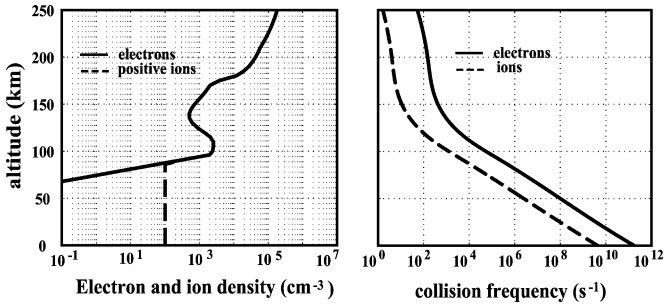

Fig. 1. Typical nighttime ionosphere profiles. Left panel: the electron density and positive ion density; right panel: the collision frequencies of electrons and ions.

II. Theory and Methods

A. Governing Equations

The ionosphere can be regarded as an inhomogeneous cold plasma with Earth's magnetic field superposed as long as the energy generated by lightning is not high enough to modify the medium. Although the electric fields produced by intense lightning discharges can modify the ionosphere, this sort of effect is localized [8], and the assumption of a linear cold plasma medium should not affect the simulation results significantly. In a cold plasma, the effect of the wave magnetic field on the charged particles and the thermal motion of the particles are neglected. All of these particles affect the electromagnetic wave behavior in the ionosphere although they do so to different degrees. In many cases, the effect caused by the ions can be neglected because the mass of an ion is about 2000 to 6000 times larger than an electron. Consequently, at ELF/VLF, the field-driven ion motion is usually much smaller than the electron motion. However, in the lowest ionosphere (below ∼60 km), the negative ion density is high compared to electrons due to the complicated chemistry processes and dominates the conductivity of the atmosphere at low altitudes. In addition, at low frequencies (∼150 Hz) close to the ion gyro-frequencies and at high altitudes (above ∼110 km), the effect of ions cannot be neglected. Hence, the contribution from ions is included in this numerical model.

The three important parameters that describe a cold magnetized plasma are.

1) Plasma frequency: $\omega_{pn} = \sqrt{q_n^2 N_n/\varepsilon_0 m_n}$, where n denotes different species of the charged particles, q_n is the charge of each type of particles, m_n is the mass of each species and N_n is the number density of the particle.
2) Gyrofrequencies: $\omega_{Bn} = |q_n B_E|/m_n$, where B is Earth's magnetic field.
3) Collision frequencies: ν_n.

Fig. 1 shows typical midlatitude density (nighttime) and collision frequency profiles of electrons and ions [3] calculated using

the International Reference Ionosphere (IRI) [28]. This ionosphere profile will be used throughout this work unless specifically stated.

The fields in this medium are described by Maxwell's equations

$$\nabla \times \mathbf{E} = -\mu_0 \frac{\partial \mathbf{H}}{\partial t} \tag{1}$$

$$\nabla \times \mathbf{H} = \varepsilon_0 \frac{\partial \mathbf{E}}{\partial t} + \mathbf{J_{tot}} \tag{2}$$

coupled to an equation for currents derived from the Lorentz equation of motion of the free electrons and ions in the medium in response to the electric field and an ambient static Earth's magnetic field

$$\frac{\partial \mathbf{J_n}}{\partial t} + \nu_{\mathbf{n}} \mathbf{J_n} = \frac{q_n}{|q_n|} \omega_{B_n} (\mathbf{J_n} \times \mathbf{b_E}) + \varepsilon_0 \omega_{pn}^2 \mathbf{E} \tag{3}$$

where $\mathbf{b_E}$ is defined as the unit vector in the direction of Earth's magnetic field and $\mathbf{J_{tot}}$ is the total currents combining the contribution from every species of charged particles, i.e., $\mathbf{J_{tot}} = \sum_n \mathbf{J_n}$.

We notice (3) is coupled to the Maxwell equations (1) and (2), resulting in a complicated but linear system describing the wave behavior in the magnetized cold plasma. The cross term from Earth's magnetic field $\mathbf{B_E}$ makes the medium anisotropic, so that the wave number depends on the wave propagation angle relative to the direction of Earth's magnetic field. This point makes the whole system challenging to implement. The coupling between the electric field, plasma electric current, and Earth's magnetic field requires the spatial and temporal averaging of many field variables, which can impact the accuracy and stability. The time derivative term in (3) describes the frequency-dependent property of the medium conductivity. As a result, the plasma currents cannot be explicitly eliminated from the equation system, which increases the number of coupled scalar equations, state variables and the numerical computation complexity.

B. Geometry and Source Current Modeling

A common and interesting (from an application stand point) form of lightning is the cloud-to-ground (CG) discharge. The current in a CG discharge is predominantly vertical. Hence, we simplify the problem from a 3-D system to 2-D cylindrical problem to substantially increase the size of problem that can be solved. The geometry of the problem is shown in Fig. 2.

Fully 3-D background magnetic fields $\mathbf{B_E}$ cannot be simulated in 2-D cylindrical coordinates. In our model, we approximate 3-D homogeneous $\mathbf{B_E}$ by taking the $\mathbf{B_E}$ along the propagation path and rotating it to make it ϕ symmetric, as demonstrated in Fig. 3 for a radial component of $\mathbf{B_E}$. The same approximation is made for any ϕ component of $\mathbf{B_E}$, and there is no need to approximate a z component because it is already ϕ symmetric. The numerical simulation results presented in later sections show that the circular symmetry approximation results in good agreement with the mode theory results, even for the near-field calculation, indicating this is a reasonable approximation.

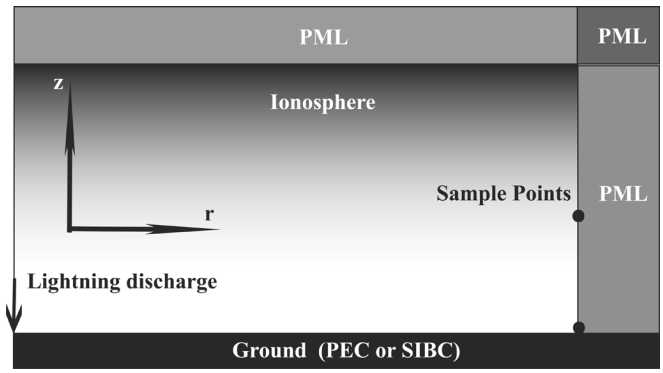

Fig. 2. Geometry of the computational domain of the FDTD model.

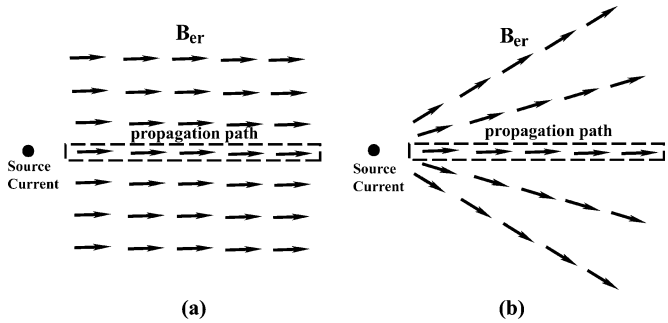

Fig. 3. Diagrams of Earth's magnetic field (only r component is shown): (a) 3-D model and (b) 2-D cylindrical model.

This model can have Earth's magnetic field $\mathbf{B_E}$ of arbitrary inhomogeneity that satisfies the ϕ symmetry constraint, but in many applications the computation domain is small enough that $\mathbf{B_E}$ is reasonably homogeneous. All simulations we show below are based on this assumption.

Lightning stroke current models are generally quite complicated [29], [30], and the FDTD approach used in this model enables a source with completely arbitrary time and spatial variations. Throughout this work, the return stroke current waveform is assumed to be uniform along the lightning discharge channel and given by

$$I(t) = I_0 \frac{\nu_0}{\gamma} \left[\exp(-at) - \exp(-bt)\right] \left[1 - \exp(-\gamma t)\right] / L \tag{4}$$

where $I_0 = 20$ kA, $\nu_0 = 8 \times 10^7$ m/s, $\gamma = 3 \times 10^4$ s^{-1}, $a = 2 \times 10^4$ s^{-1}, $b = 2 \times 10^5$ s^{-1}, and L is the lightning discharge channel length [31].

III. Technique Details

A. Finite Difference Algorithm and Discretization Scheme

Several FDTD methods have been developed to address the issue of electromagnetic wave propagation in a cold plasma. Nickisch and Franke [32] proposed a method that is unstable if the plasma has nonzero collision frequency [33]. Young [34] derived a method with a differencing scheme in which H and J are collocated in time. This method results in an efficient set of iterative equations that have a fairly simple structure even for complicated anisotropy. However, the main limitation of this method is that the maximum Courant number is $\sqrt{1 - (\omega_{pn}\Delta t/2)^2}$ and

is dependent on the particle plasma frequency. In our application, this can result in an extremely small time step at high altitude to ensure the stability of the whole system. Another class of FDTD method for cold plasma is the recursive convolution (RC) methods. The original RC method [35] is only first order accurate [33], [34]. The improved RC method piecewise linear recursive convolution (PLRC) [36] is second order accurate but its stability condition is also dependent on medium properties [33].

In consideration of these properties, we adopt the direct integration (DI) FDTD [33] method. This method collocates E and J in time and space, which results in a more tightly coupled and complicated set of difference equations. The most appreciable advantage of $E-J$ method is that the stability condition in unmagnetized plasma is independent of medium properties and remained the same as free space. We find empirically that this is also valid for magnetized plasma. We can quantify this advantage by considering the stability condition for 1D problem without the presence of Earth's magnetic field. For a typical ionosphere profile shown in Fig. 1, at 200 km above the ground, the plasma frequency is about 1.13×10^{7} rad/s. Consequently, the maximum time step for $H-J$ method is 1.76×10^{-7} s based on the maximum Courant number defined as $\sqrt{1-(\omega_{pn}\Delta t/2)^2}$. The maximum time step size for the $E-J$ method is not dependent on the plasma frequency and remained the same as in free space, which is about 1.67×10^{-6} s if the spatial step size is chosen to be 0.5 km. This value is almost one order larger than that of the $H-J$ method.

B. Iteration Coefficients

Considering the three species of particles (electrons, positive ions, and negative ions), the whole system can be converted to 15 scalar equations with 15 state variables. After the discretization of these equations using $E-J$ collocation, these 15 equations can be divided into two groups. The first group consists 12 linear equations and the corresponding 12 state variables are all the components of $\mathbf{E}$ and $\mathbf{J}$, which can be written as

$$AX^n = BX^{n-1} + CY^{n-1/2} \tag{5}$$

where

$$X^n = \left[E_r^n\ E_\phi^n\ J_{r\_e}^n\ J_{r\_ip}^n\ J_{r\_in}^n\ J_{\phi\_e}^n\ J_{\phi\_ip}^n\ J_{\phi\_in}^n\ E_z^n\ J_{z\_e}^n\ J_{z\_ip}^n\ J_{z\_in}^n\right]^T$$

and

$$Y^{n-1/2} = \left[\frac{\partial H_{phi}^{n-1/2}}{\partial z}\ \frac{\partial H_r^{n-1/2}}{\partial z}\ \frac{\partial H_z^{n-1/2}}{\partial r}\ \frac{\partial H_{phi}^{n-1/2}}{\partial r}\ \frac{H_{phi}^{n-1/2}}{r} J_s\right]^T.$$

$A(12\times12)$, $B(12\times12)$ and $C(12\times6)$ are the coefficient matrixes that depend on the medium properties and discretization parameters.

To derive an explicit set of difference equations, we need to solve for all the state variables simultaneously. Analytical deriving the coefficients for FDTD iteration equations ($E-J$ collocated) means solving a linear equation system of 12th order. This kind of symbolic calculation is very tedious and complicated even with the aid of a symbolic calculation package such as *Maple* or *Mathematica* because the matrixes are not block diagonal thus the closed form of these coefficients are very complicated. An alternative way to do this is deriving the difference equation coefficients numerically with the equation given by

$$X^n = (A^{-1}B)X^{n-1} + (A^{-1}C)Y^{n-1/2}. \tag{6}$$

The entries in $(A^{-1}B)$ and $(A^{-1}C)$ are all the coefficients needed to implement the explicit FDTD iteration and these coefficients are only needed to be calculated once for a time invariant system. The coupling of the 12 linear equations and the leapfrog scheme make spatial averaging necessary during implementing the whole system. For example, to update E_r, we need to use the state variables E_ϕ, E_z, J_ϕ, J_z, H_ϕ and the derivative $\partial H_\phi/\partial z$, $\partial H_r/\partial z$, $\partial H_\phi/\partial r$, which are not spatially collocated with E_r. The whole equation system can be built by combining (5) and the second group of three difference equations for the H update, which is easy for coding and reduces the computational complexity.

One point need to be mentioned for this method is that the field values have to be scaled to avoid ill conditioning of the coefficient matrixes A and B. The scaling scheme is shown as below

$$\breve{H} = \frac{\mu_0\Delta z}{\Delta t}H \tag{7}$$

$$\breve{J} = \frac{\Delta t}{\varepsilon_0}J. \tag{8}$$

In the above formula, $\breve{H}$ and $\breve{J}$ are the scaled field values to be used in iteration while H and J are the original field values. The electric field in this scheme has no need to be scaled. By doing this, the extremely huge original condition numbers (around 10^{16}) of the iteration coefficient matrixes can be reduced to acceptable numbers (around 10^5) to avoid the stability and accuracy problems.

C. Absorbing Boundary Condition

In this electromagnetic wave propagation model, ABCs are always required to truncate the computational domain without artificial reflections at the outer boundaries. Few ABCs are capable of handling a strongly dispersive and anisotropic medium such as cold plasma. The perfectly matched layer [37] is one that can handle such a medium [38], [39]. We use the NPML variant [25] for ease of implementation.

Following Cummer [25], the governing equations of the NPML for the transverse magnetic (TM) fields (E_r, E_z, H_ϕ) are

$$i\omega\varepsilon_0 E_r = -\frac{\partial}{\partial z}\bar{H}_\phi^z = -\frac{\partial}{\partial z}\left(\frac{H_\phi}{1-i\sigma_z/\omega}\right) \tag{9}$$

$$i\omega\varepsilon_0 E_z = \frac{\partial \bar{H}_\phi^r}{\partial r} + \frac{\bar{H}_\phi^{\bar{r}}}{r} = \frac{\partial}{\partial r}\left(\frac{H_\phi}{1-i\sigma_r/\omega}\right) + \frac{1}{1-i\sigma_{\bar{r}}/\omega}\frac{H_\phi}{r} \tag{10}$$

$$i\omega\mu_0 H_\phi = \frac{\partial \bar{E}_z^r}{\partial r} - \frac{\partial \bar{E}_r^z}{\partial z} = \frac{\partial}{\partial r}\left(\frac{E_z}{1 - i\sigma_r/\omega}\right) - \frac{\partial}{\partial z}\left(\frac{E_r}{1 - i\sigma_z/\omega}\right) \quad (11)$$

where σ_r and σ_z are NPML conductivities in r and z direction and $\sigma_{\bar{r}} = (1/r)\int_0^r \sigma(s)ds$. The TE fields in the NPML obey similar equations.

The primary advantage of the NPML formulation is that the NPML partial differential system is in the exact same form as the regular medium equation system with the replacement of those unstretched variables by stretched variables. The relationship between the stretched variables and the unstretched variables is simply defined by the ordinary differential (12) coupled to the original equation system, which is easy to be converted to the time domain form

$$\bar{F}^\xi = \frac{F}{1 - i\sigma_\xi/\omega} \quad (12)$$

where $F \in \{H_\phi, E_r, E_z\}$ and $\xi \in \{r, z, \bar{r}\}$.

This point makes the NPML very flexible in practical applications because it can be applied to different numerical methods without changing the primary iterative equations. This is a significant advantage in a complex medium because the derivation of difference equation coefficients is time consuming and tedious. The NPML has been proved to be a true perfectly matched layer in Cartesian coordinates and have similar performance to the standard PML in curvature coordinates [40].

D. Air-Ground Interface

Previous FDTD models have treated the ground as a perfect electric conductor (PEC) [19], [20]. But, in reality, ground is a lossy dielectric and at higher VLF frequencies, this property becomes important. Due to this fact, very small cell size is required if we need to model the wave propagation in the ground accurately. For example, if the conductivity of the ground is 0.01 S/m, the permittivity is 15 and the permeability is 1, which are reasonable parameters for the ground, to accurately calculate a 5 kHz wave propagating in the ground, the maximum space step we can choose is approximately 45 m to maintain 10 sample points per wavelength. Such small cell size results in a huge number of cells for the computational domain of many applications. Therefore, directly applying FDTD method on the lossy ground is unacceptable in consideration of the current limitation of computer power and memory.

Since we are not interested in the fields below the ground surface in this work, if we can treat the interface between the atmosphere and the lossy ground correctly without calculating the fields inside the ground, a significant computational saving can be achieved. The technique of surface impedance boundary conditions (SIBC) [26], [27] is a good choice here although this method is an asymptotic method. The idea of SIBC is finding the relationship between the tangential electric fields and the tangential magnetic fields at the interface. In frequency domain, the relation is given by

$$E_\phi(\omega) = H_r(\omega) \cdot Z_{sh}(\omega) \quad (13)$$

$$E_r(\omega) = -H_\phi(\omega) \cdot Z_{sv}(\omega) \quad (14)$$

where $Z_{sv}(\omega)$ and $Z_{sh}(\omega)$, both of which depend on the transmission angle θ_t with the expression of

$$\theta_t = \cos^{-1}\left[\sqrt{1 - \frac{sin^2\theta_i}{\mu_r\varepsilon_r\left(1 - \frac{i\sigma}{\omega\varepsilon_0\varepsilon_r}\right)}}\right] \quad (15)$$

are the surface impedance of the lossy ground for vertical and horizontal polarizations respectively. Given the low frequencies of interest, we assume $\sigma/\omega\varepsilon_0\varepsilon_r \gg 1$, which means whatever the incident angle is, the transmission angle is always very close to 90°. In other words, the ground is not a perfect electric conductor (PEC) but a good conductor for the frequency range we are interested in and this fact makes the radio wave arriving the interface enter the ground nearly normally independent of the incident angle.

Consequently, the surface impedances for these two polarizations are approximately the same

$$Z_{sv}(\omega) \approx Z_{sh} \approx \sqrt{\frac{i\omega\mu_0}{i\omega\varepsilon + \sigma}} \approx \sqrt{\frac{i\omega\mu_0}{\sigma}} = Z_s(\omega). \quad (16)$$

Let $Z_s' = Z_s(\omega)/i\omega = \sqrt{\mu_0/i\omega_0}$, we have

$$E_\phi(t) = Z_s' * \left[\frac{\partial}{\partial t} H_r(t)\right]. \quad (17)$$

To save the computational expense, we need to implement the above convolution of SIBC recursively. This can be achieved by the exponential fitting of the discrete impulse response. Then, only two time levels of H_r are needed for the approximation of the convolution. Very similar equations can be derived for the other polarization.

E. Earth Curvature Approximation

For short distance propagation with small incident angles, Earth curvature can be neglected. However, the effect of Earth curvature is significant when the incident angle of the propagation exceeds 50° to 60° [41] or the frequency is higher than ~12 kHz. Therefore, the Earth-flattening approximation has to be used in this work. There are several methods available for Earth curvature correction. One of the most convenient is the method of the modified refractive index [41], [42]. The essence of this method is to replace the larger physical distance of the upper layers of the ionosphere by a larger electrical distance by introducing a fictitious refractive index correction factor. That is $n_m(z) = n \cdot f_m(z)$, where $f_m(z) = (1 + z/r_0)$, r_0 is the radius of Earth and z is the height. Please be noted that this is only correct when $z \ll r_0$, i.e. the thin shell case. This method of Earth curvature correction is derived from the Bouger law by ray theory. Other methods such as the conformal mapping earth flattening procedures [43] result in similar formulations.

To apply this method in this full wave FDTD model, we scale the different field components in different ways. Namely, we scale the permeability for the TM mode fields (H_z, E_r, E_ϕ) and the permittivity for the TE mode fields (E_z, H_r, H_ϕ) to keep the total magnetic energy and electric energy unchanged after introducing the fictitious refractive index factors.

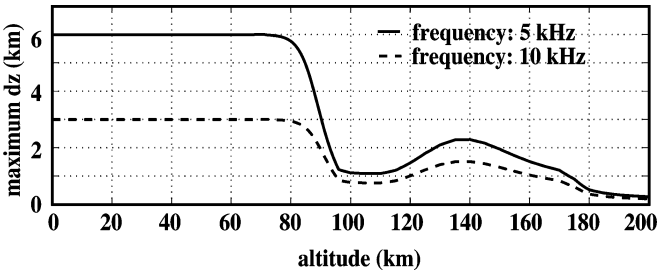

Fig. 4. Maximum cell size profiles versus altitudes for the specific source frequencies.

F. Dispersion Analysis

In a cold plasma with the presence of a static magnetic field, the dispersion relation is dependent on the wave propagation direction because the medium is anisotropic. Another important property of this medium is that two propagation modes exist, the ordinary mode (*O*-mode) and extraordinary mode (*X*-mode). With the aid of the dispersion relation analysis, given the ionosphere profiles, error tolerance, propagation direction and the frequency range, we can estimate the maximum spatial grid size Δz as a function of altitude. This analysis is helpful to estimate the numerical simulation accuracy.

At low altitudes, the electron density is not very high, thus the wave propagation pattern is not very different from free space. But at high altitudes, due to the alignment effect of Earth's magnetic field, the wave propagates nearly vertically. Because of this, here we consider a vertically propagating wave for the accuracy analysis. We assume Earth's magnetic field is vertical and homogeneous with the magnitude of 5×10^{-5} T. By requiring that Δz is at most 1/10 of a wavelength, Fig. 4 shows the maximum possible Δz as a function of altitude. The *X*-mode has the larger real part of refractive index and thus shorter wavelength, hence the analysis is based on this mode. Based on the dispersion analysis results, the maximum Δz we can use is 270 m for the frequency of 5 kHz and 190 m for the frequency of 10 kHz if the maximum altitude is 200 km. If we want to use $\Delta z = 1$ km in the simulations, then we can ensure the accuracy up to 5 kHz and the maximum altitude should not exceed 175 km.

The result shown in Fig. 4 is just a rough estimate of the grid size we can choose, which is used as a reference for choosing the parameters of the simulations. In implementation of this model, we may need to adjust the spatial grid size around this reference value to meet the specific accuracy requirements. The accumulated error of the electromagnetic fields at a specific location is dependent on the propagation paths, which is not easy to be evaluated accurately. We will examine the solution convergence of this FDTD model in later sections.

IV. Numerical Results and Discussions

A. Comparison With Mode Theory

Here we consider three typical cases to examine the accuracy of this FDTD model by comparing with the mode theory results. Earth's magnetic field with the magnitude of 5×10^{-5} T is in z, r and ϕ direction for these three cases respectively. The spatial grid size is chosen as 1 km. The observation point is located at the ground level and 300 km away from the source current. The ionosphere is the typical nighttime profile which is shown in Fig. 1. The numerical mode theory solution was obtained by using the LWPC [13]. Fig. 5 shows the numerical results of this FDTD model and mode theory model. In the upper panel and the middle panel of Fig. 5 (note the nonlinearity of the horizontal axis), the FDTD simulation results are in good agreement with the mode theory results. The errors of B_{ez} and B_{er} cases are -3.9% and 0.2%, respectively. The error is defined as $(\sum_f |\widetilde{B}_{\rm FDTD}| - \sum_f |\widetilde{B}_{\rm ref}|)/\sum_f |\widetilde{B}_{\rm ref}|$, where $\widetilde{B}_{\rm FDTD}$ is the frequency spectrum of this FDTD model solution and $\widetilde{B}_{\rm ref}$ is the LWPC results, which is regarded as the reference solution. The summation is implemented in the frequency range from 0 to 30 kHz. In the case where Earth's magnetic field is aligned in ϕ direction, the error (-18%) is bigger than the other two cases, as shown in the lower panel of Fig. 5. However, we still find these two simulation results are very close up to 6 kHz with the error around -0.7%. In general, the mode theory solutions have more frequency variability at higher frequencies, which implies higher order modes with lower loss than FDTD predicts. The source of this small discrepancy is difficult to determine because both models are numerical and no exact solution to this problem exists. This discrepancy occurs for the case where the background magnetic field is purely vertical and no approximation is made about the background field geometry (see Fig. 3), thus this approximation is not the error source. We also note that, as will be shown later, the FDTD solution appears to have converged to the error of less than a few percent, suggesting that the FDTD solution is correct and perhaps the mode theory solution is not. In either case, the good agreement between these two completely different numerical techniques indicates that both are correctly solving the problem.

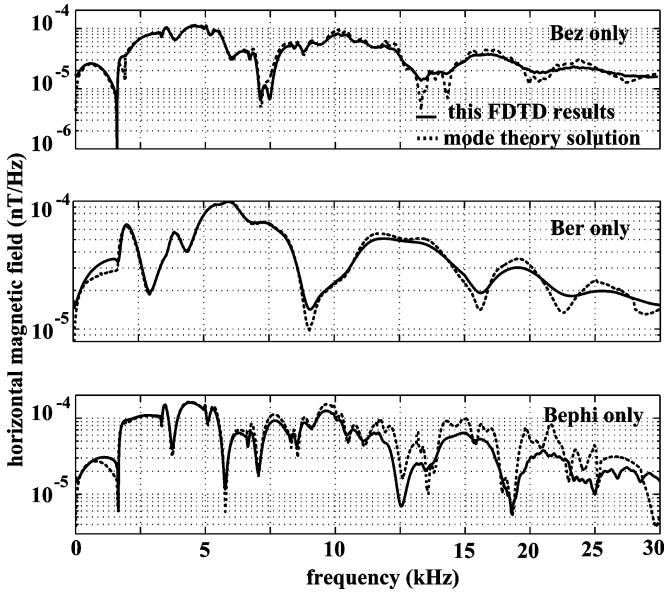

Fig. 5. Comparison between the numerical simulation results of this FDTD model and mode theory solutions. Upper panel: Earth's magnetic field is vertical; middle panel: Earth's magnetic field is in r direction; lower panel: Earth's magnetic field is in ϕ direction.

Fig. 6 shows the effect of Earth curvature correction. Earth's magnetic field is still assumed to be 5×10^{-5} T. The codip angle is 20° and the magnetic azimuth angle (horizontal Earth's

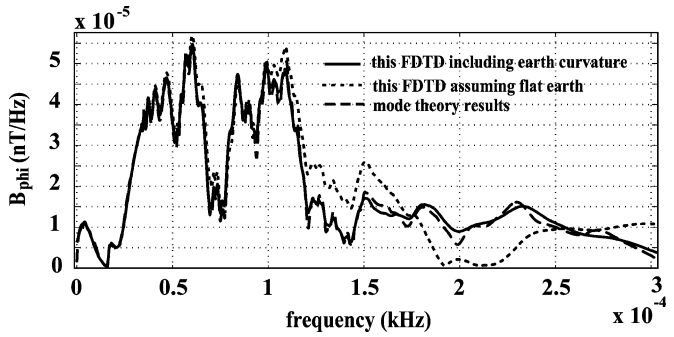

Fig. 6. Comparison between the mode theory solutions, this FDTD model including the Earth curvature correction, and this FDTD model assuming flat ground.

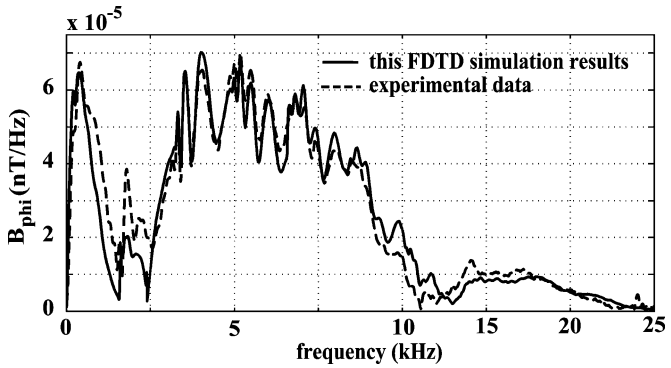

Fig. 7. Comparison between the experimental data collected by the ELF/VLF measurement system and this FDTD simulation results. The Earth curvature correction is included in the FDTD model.

magnetic field to the wave propagation direction k) is 90°, i.e. $B_{ez} = -4.70 \times 10^{-5}$ T, $B_{er} = 0$, and $B_{e\phi} = 1.71 \times 10^{-5}$ T. The electron density profile is defined as [44], [45]

$$N_e(h) = 1.43 \times 10^{13} \exp(-0.15h') \exp\left[(\beta - 0.15)(h - h')\right] \tag{18}$$

where $\beta = 0.5\ \mathrm{km}^{-1}$ and $h' = 84.2$ km are obtained by ionosphere remote sensing [1]. The relative permittivity and the conductivity of the ground are 10 and 0.01 S/m, respectively. The distance between the transmitter and the receiver is 894 km. All of these parameters are from the experimental data although the measured data are not shown here. We will compare our simulation results with the experimental data later in another example. As expected, we find Earth curvature has little effect on the simulation results for low frequency components (below 12 kHz) but the assumption of flat ground leads to substantial errors for high frequency waves. After the correction, this error was compensated very well and the FDTD model simulation results and the mode theory results are very close in a wide frequency range up to 30 kHz. It is important to include this correction factor for all but the shortest distance (<200 km) and lowest frequency (<10 kHz) simulations.

B. Comparison With Experimental Data

This FDTD model will be used for lightning-generated electromagnetic wave propagation prediction and ionospheric or lightning remote sensing applications. Here, the simulation results of this FDTD model are compared with the experimental data collected by an ELF/VLF sensor at Duke University between 04:14:07.327 and 04:42:43.167 UT, JD 196 (July 14), 2004. We selected those lightning in a small region whose latitude and longitude are from 35.1408° to 36.0552° and −72.1942° to −72.0102°, respectively, which were obtained from the National Lightning Detection Network (NLDN). This process is important because, by confining the lightning sources in this small region, we can ensure the sferics radiated by these lightning discharges were propagating through the same path with the same ionosphere condition. In total 10 sferics with good SNR launched by the corresponding negative lightning discharges were chosen for the comparison. Then, we accurately aligned these ten waveforms in time domain and conducted averaging on them to improve the SNR. The first 20 ms of these sferic waveforms were included in the averaging procedure in order to cover the wide frequency range we are interested in. The propagation distance (629 km) and the azimuth angle (280°) can be determined accurately using the NLDN data. The codip angle is 20°. Earth's magnetic field is again 5×10^{-5} T. Thus, $B_{ez} = -4.70 \times 10^{-5}$ T, $B_{er} = 2.97 \times 10^{-6}$ T and $B_{e\phi} = -1.68 \times 10^{-5}$ T. The permittivity and the conductivity of the ground are 81 and 4 S/m (sea water). The parameters of the electron density profile is again defined by [18] with $\beta = 0.45\ \mathrm{km}^{-1}$ and $h' = 85.6$ km. An eight-pole low pass filter with the cutoff of 25 kHz was applied on both the experimental data and the simulation results. The FDTD simulation results was multiplied by the frequency response of the ELF/VLF antenna $H = 0.81 \cdot j\omega/[\omega_0(1 + j\omega/\omega_0)] \cdot 1/(1 + j\omega/\omega_1)$ to compare with the experimental data, where $\omega_0 = 100 \cdot 2\pi$ rad/s and $\omega_1 = 13 \times 10^3 \cdot 2\pi$ rad/s. The frequency spectra of the received sferics and this FDTD simulation results are shown in Fig. 7. The source used here in this simulation is given by

$$I(t) = \begin{cases} 0, & \text{for } t < 0 \\ \sum_k I_k \exp\left(-\frac{t}{t_k}\right), & \text{for } t \geq 0 \end{cases} \tag{19}$$

where $k = 4$, $I_1 = 20$ kA, $I_2 = -20$ kA, $I_3 = 12$ kA, $I_4 = -12$ kA, $t_1 = 50\ \mu$s, $t_2 = 5\ \mu$s, $t_3 = 333\ \mu$s and $t_4 = 5\ \mu$s.

In Fig. 7, the spectrum of the FDTD simulation result matches the experimental data very well. The error is defined as $(\sum_f |\widetilde{B}_{\mathrm{FDTD}}| - \sum_f |\widetilde{B}_{\mathrm{data}}|)/\sum_f |\widetilde{B}_{\mathrm{data}}|$, where $\widetilde{B}_{\mathrm{FDTD}}$ is the frequency spectrum of this FDTD model result and $\widetilde{B}_{\mathrm{data}}$ is the frequency spectrum of the measured horizontal magnetic field. The error over the frequency range up to 30 kHz is within 5%. The possible reasons causing the slight differences between them are: 1) The ionosphere profiles used in FDTD simulation could not be exactly the same as the real ionosphere status at the time when lightning discharges occurred; 2) The source current we used in the FDTD simulation is different from the real source; 3) Earth's magnetic field in the simulation is homogeneous, which is not the real case, although for east-west propagation path this approximation is reasonable. In light of these uncertainties that prevent a perfect comparison with experimental data, the agreement between the model and data is very strong.

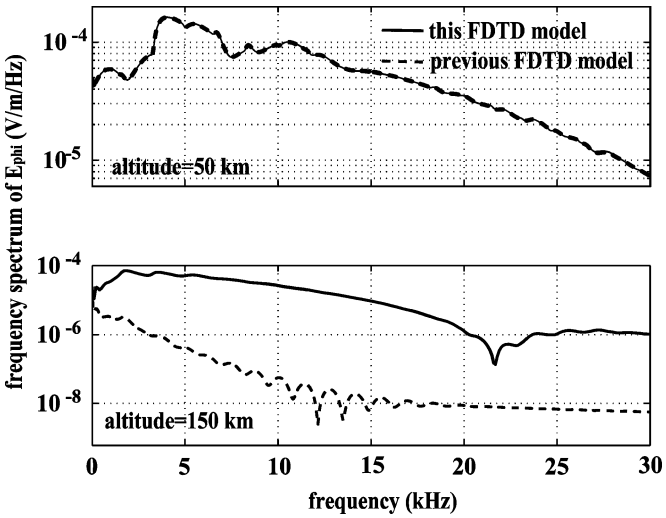

Fig. 8. Comparison between simulation results of this FDTD model and the previous model with the simple conductor approximation at low and high altitudes. Upper panel: the altitude is 50 km; Lower panel: the altitude is 150 km.

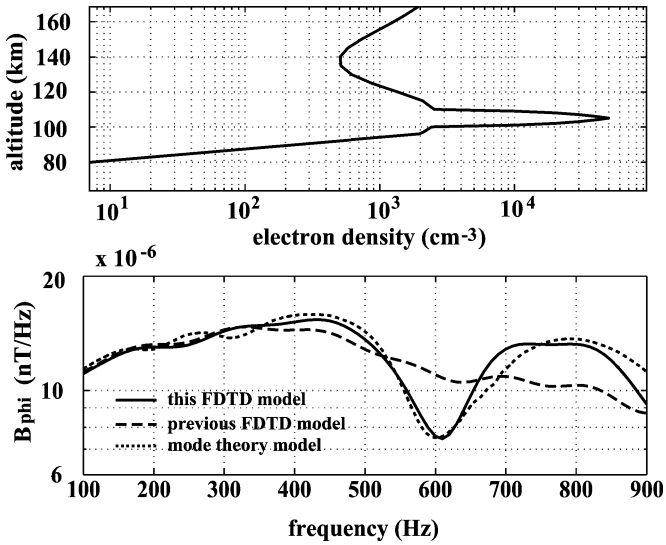

Fig. 9. Numerical simulation results with the presence of an Es layer. Upper panel: the electron density profile with an Es layer; lower panel: the comparison between the simulation results of the previous FDTD model with the simple conductor approximation, this FDTD model, and the mode theory model. The spatial grid size is 0.5 km for the FDTD models.

C. High Altitude Fields

Some of the previous models [19], [20] are based on an approximation of (3). These models assume that the wave frequency is much lower than particles' collision frequencies. Thus, the first item in (3) can be neglected and the cold plasma can be approximated by a medium with the equivalent anisotropic frequency independent conductivity. This assumption simplifies the iteration equations and saves the computational cost significantly. However, this assumption is not valid at high altitudes where the collision frequencies of particles are quite low, which is evident in Fig. 1. The comparison between the previous models using the simple conductor approximation and this FDTD model both in low altitude and high altitude is plotted in Fig. 8.

E_ϕ at the altitude of 50 km above the ground calculated by the previous model is observed to be indistinguishable from this FDTD model. However, at 150 km above the ground, the previous model results in ~40 to 60 dB weaker E_ϕ than this FDTD model results over the frequency range from 5 to 30 kHz. Observing (3), we find the assumption made in the previous model means that the first term on the LHS of (3) is omitted, which leads to larger plasma currents for a fixed value of electric field compared with this FDTD model, i.e. the assumption that the wave frequency is much lower than particles' collision frequencies introduces more loss at high altitudes. This FDTD model is more accurate than the previous models in high altitude regions because this assumption was removed in this model.

The importance of correctly treating the medium at high altitudes is also evident in the low altitude fields under some conditions. For example, the ionosphere profile shown in Fig. 9 is associated with a sporadic E layer (Es), a transient layer in the E region of the ionosphere with relatively high electron density, which affects the wave propagation at altitudes where the conductor approximation is not valid. We use this ionosphere profile with the Es layer as the input of the two FDTD models to calculate the magnetic field 600 km away from the source current. The cell size is chosen as 0.5 km for both FDTD models due to the enhancement of the electron density in the E_s layer. The results are no longer same for these two different FDTD models as shown in the lower panel of Fig. 9.

There is a strong attenuation maximum around 600 Hz in this FDTD model simulation results and mode theory solution. However, in the previous FDTD model results, no such characteristics are found. This strong attenuation maximum is contributed from a resonance phenomenon caused by the Es layer [2]. The depth and frequency of this attenuation maximum are dependent on the altitude and maximum of the electron density of the Es layer [46]. To model this effect correctly, a full plasma treatment of the ionosphere is clearly required.

D. Accuracy Convergence

We have conducted the general accuracy analysis by the dispersion analysis. Here we are going to examine the error convergence of this FDTD model. Without losing generality, we reran the case in the upper panel of Fig. 5 with the same parameters but different cell sizes (4, 2, 1, and 0.5 km) to investigate the solution convergence for different frequencies. We regard the simulation results with $\Delta z = 0.5$ km as the reference, then computed the relative errors of the other simulation results and plotted the errors in Fig. 10.

In Fig. 10, the errors of $\Delta z = 4$ km case seriously deviate from the other cases. This is reasonable because it is very likely that $\Delta z = 4$ km is too big to resolve the high frequency components or the rapidly increasing electron density at high altitudes. For $\Delta z = 1$ km case, all the errors are within 5% for frequency up to 30 kHz. In the range from 0 to ~20 kHz, the error of $\Delta z = 1$ km is controlled within 2.5%. The expected second order convergence of the model implies that it is reasonable to take $\Delta z = 0.5$ km solution as the reference value. From $\Delta z = 4$ km to $\Delta z = 1$ km, the solution converges quickly and the solution of $\Delta z = 1$ km case is very close to the reference. For lower frequency applications, we may use larger cell size. For example, we find that, if $\Delta z = 2$ km, the solution error is

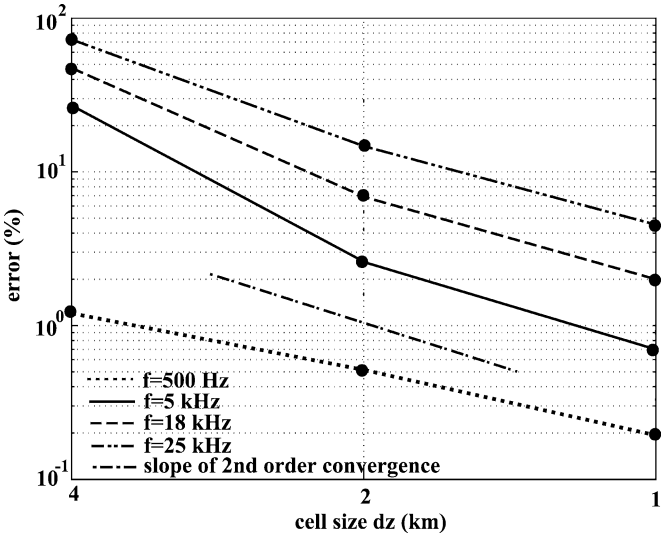

Fig. 10. Convergence of solution of this FDTD model solutions: the absolute value of the relative errors of this FDTD model with different cell sizes (0.5, 1, 2, and 4 km). The solution of $\Delta z = 0.5$ km case is regarded as the reference value.

as low as 6% for the frequency up to 10 kHz. The straight dash doted line in Fig. 10 represents the slope of second order convergence. Evidently, the error convergence lines for various frequency components from $\Delta z = 2$ km to $\Delta z = 1$ km are almost parallel to this dash doted line, which validates that this model is second order accurate. Note that the error of this model is dependent on the ionosphere profile, but because we have chosen a realistic profile for this analysis, we expect the convergence in other realistic cases to be similar.

V. Conclusion

We have developed a 2-D cylindrical FDTD model for lightning-generated electromagnetic wave simulation that treats the ionosphere as a true cold plasma including the effects from various charged particles and it is capable of using arbitrary ionosphere profiles, arbitrary background magnetic fields, and arbitrary source current waveforms. After comparing the advantages and disadvantages of different techniques for treating the cold plasma in an FDTD simulation, we find the $E - J$ method is preferable in consideration of the computational expense. This method increases the complexity of coefficient matrix derivation, but numerically deriving the explicit FDTD iteration coefficients simplifies the tedious analytical computation and difficulties in implementation. The NPML ABC used in this model works well and its performance is equivalent to other versions of PML while the NPML is simpler to implement in the complex medium considered here. The SIBC is used in this FDTD model in treating the air-ground interface to make the model more efficiently. The method of modified refractive index for Earth curvature correction included in this FDTD model reduces the error significantly for high frequency (above $\sim$10 kHz) components and long distance ($>$200 km) propagation without any extra computational expense.

The general accuracy requirements can be met by carefully choosing the cell size and maximum altitude of the computational domain based on the dispersion analysis. The numerical results of this FDTD model agree with a numerical mode theory model very well with the agreement between the models better than 5% over the frequency range from 0 to 30 kHz for typical nighttime ionosphere profiles with the vertical Earth's magnetic field in presence. Convergence analysis of the FDTD model shows that it has converged to approximately 1% error when $\Delta z = 1$ km, suggesting that this difference might be caused by the errors in the mode theory solution.

Although previous FDTD models simplify the original equation system and generate almost the same results as this model at the ground level for typical nighttime ionosphere profiles, those models with the simple conductor approximation introduce extra energy loss (40$\sim$60 dB) at high altitudes thus result in large errors at high altitudes. Furthermore, this FDTD model can simulate the wave propagation correctly under some special circumstances like the ionosphere with a sporadic E layer (Es). The strong agreement between the FDTD simulation results and the experimental data recorded by the ELF/VLF measurement systems validates this model and highlights its potential in future ionospheric remote sensing and other geophysical applications.

References

[1] S. A. Cummer, U. S. Inan, and T. F. Bell, "Ionospheric D region remote sensing using VLF radio atmospherics," *Radio Sci.*, vol. 33, pp. 1781–1792, 1998.

[2] S. A. Cummer and U. S. Inan, "Ionospheric E region remote sensing with ELF radio atmospherics," *Radio Sci.*, vol. 35, pp. 1437–1444, 2000.

[3] ——, "Modeling ELF radio atmospheric propagation and extracting lightning currents from ELF observations," *Radio Sci.*, vol. 35, pp. 385–394, 2000.

[4] W. Hu, S. A. Cummer, W. A. Lyons, and T. E. Nelson, "Lightning charge moment changes for the initiation of sprites," *Geophys. Res. Lett.*, vol. 29, no. 8, p. 1279, 2002.

[5] R. C. Franz, R. J. Nemzek, and J. R. Winckler, "Television image of a large electrical discharge above a thunderstorm system," *Science*, vol. 249, pp. 48–51, 1990.

[6] V. P. Pasko, U. S. Inan, T. F. Bell, and Y. N. Taranenko, "Sprites produced by quasielectrostatic heating and ionization in the lower ionosphere," *J. Geophys. Res.*, vol. 102, no. A3, pp. 4529–4561, 1997.

[7] V. P. Pasko, U. S. Inan, and T. F. Bell, "Mesospheric electric field transients due to tropospheric lightning discharges," *Geophys. Res. Lett.*, vol. 26, pp. 1247–1250, 1999.

[8] Y. N. Taranenko, U. S. Inan, and T. F. Bell, "Interaction with the lower ionosphere of electromagnetic pulses from lightning: heating, attachment, and ionization," *Geophys. Res. Lett.*, vol. 20, pp. 1539–1542, 1993.

[9] R. A. Roussel-Dupré and A. V. Gurevich, "On runaway breakdown and upward propagating discharges," *J. Geophys. Res.*, vol. 101, pp. 2297–2311, 1996.

[10] K. G. Budden, *The Wave-Guide Mode Theory of Wave Propagation*. London, U.K.: Logos Press, 1961.

[11] J. R. Wait, *Electromagnetic Waves in Stratified Media*. Oxford, U.K.: Pergamon Press, 1970.

[12] J. Galejs, *Terrestrial Propagation of Long Electromagnetic Waves*. Oxford, U.K.: Pergamon Press, 1972.

[13] J. A. Ferguson, F. P. Snyder, D. G. Morfitt, and C. H. Shellman, Long-wave Propagation Capability and Documentation, Tech. Doc., Naval Ocean Systems Center, San Diego, CA, 1989.

[14] A. Taflove, *Computational Electromagnetics: Finite-Difference Time-Domain Method*. Boston, MA: Artech House, 1995.

[15] R. A. Pappert and J. A. Ferguson, "VLF/ELF mode conversion model calculations for air to air transmission in the earth-ionosphere waveguide," *Radio Sci.*, vol. 21, pp. 551–558, 1986.

[16] M. Cho and M. J. Rycroft, "Computer simulation of the electric field structure and optical emission from cloud-top to the ionosphere," *J. Atoms. Terr. Phys.*, vol. 60, pp. 871–888, 1998.

[17] V. P. Pasko, U. S. Inan, T. F. Bell, and S. C. Reising, "Mechanism of ELF radiation from sprites," *Geophys. Res. Lett.*, vol. 25, pp. 3493–3496, 1998.

[18] G. Veronis, V. P. Pasko, and U. S. Inan, "Characteristics of mesospheric optical emissions produced by lightning discharges," *J. Geophys. Res.*, vol. 104, pp. 12 645–12 656, 1999.
[19] Z. Ma, C. L. Croskey, and L. C. Hale, "The electrodynamic responses of the atmosphere and ionosphere to the lightning discharge," *J. Atoms. Terr. Phys.*, vol. 60, pp. 845–861, 1998.
[20] S. A. Cummer, "Modeling electromagnetic propagation in the Earth-ionosphere waveguide," *IEEE Trans. Antennas Propag.*, vol. 48, pp. 1420–1429, 2000.
[21] M. Thèvenot, J. P. Bérenger, T. Monedière, and F. Jecko, "A FDTD scheme for the computation of VLF-LF propagation in the anisotropic earth-ionosphere waveguide," *Ann. of Télécommun.*, vol. 54, pp. 297–310, 1999.
[22] T. Otsuyama, D. Sakuma, and M. Hayakawa, "FDTD analysis of ELF wave propagation and Schumann resonances for a subionospheric waveguide model," *Radio Sci.*, vol. 38, no. 6, p. 1103, 2003.
[23] J. J. Simpson and A. Taflove, "Three-dimensional FDTD modeling of impulsive ELF propagation about the Earth-sphere," *IEEE Trans. Antennas Propag.*, vol. 52, pp. 443–451, 2004.
[24] H. Yang and V. P. Pasko, "Three-dimensional finite difference time domain modeling of the Earth-ionosphere cavity resonances," *Geophys. Res. Lett.*, vol. 32, p. L03114, 2005.
[25] S. A. Cummer, "A simple, nearly perfectly matched layer for general electromagnetic media," *IEEE Microw. Wireless Lett.*, vol. 13, pp. 128–130, 2003.
[26] J. G. Maloney and G. S. Smith, "The use of surface impedance concepts in the finite-difference time-domain method," *IEEE Trans. Antennas Propag.*, vol. 40, pp. 38–48, 1992.
[27] S. Kellali, B. Jecko, and A. Reineix, "Implementation of a surface impedance formalism at oblique in FDTD method," *IEEE Trans. Electromagn. Compat.*, vol. 35, pp. 347–356, 1993.
[28] D. Bilitza, "International reference ionosphere—status 1995/96," *Adv. Space Res.*, vol. 20, pp. 1751–1754, 1997.
[29] M. A. Uman, *The Lightning Discharge*. Orlando, FL: Academic Press, 1987.
[30] R. Thottappillil, V. A. Rakov, and M. A. Uman, "Distribution of charge along the lightning channel: relation to remote electric and magnetic fields and to return-stroke models," *J. Geophys. Res.*, vol. 102, no. D6, pp. 6987–7006, 1997.
[31] A. S. Dennis and E. T. Pierce, "The return stroke of the lightning flash to Earth as a source of VLF atmospherics," *Radio Sci.*, vol. 68D, p. 777, 1964.
[32] L. J. Nickisch and P. M. Franke, "Finite-difference time-domain solution of Maxwell's equations for the dispersive ionosphere," *IEEE Antennas Propag. Mag.*, vol. 34, pp. 33–39, 1992.
[33] S. A. Cummer, "An analysis of new and existing FDTD methods for isotropic cold plasma and a method for improving their accuracy," *IEEE Trans. Antennas Propag.*, vol. 45, pp. 392–400, 1997.
[34] J. L. Young, A. Kittichartphayak, Y. M. Kwok, and D. Sullivan, "On the dispersion errors related to $(\mathrm{FD})^2\mathrm{TD}$ type schemes," *IEEE Trans. Microw. Theory Tech.*, vol. 43, pp. 1902–1909, 1995.
[35] R. J. Luebbers, F. Hunsberger, and K. S. Kunz, "A frequency-dependent finite-difference time-domain formulation for transient propagation in a plasma," *IEEE Trans. Antennas Propag.*, vol. 39, pp. 29–34, 1991.
[36] D. F. Kelley and R. J. Luebbers, "Piecewise linear recursive convolution for dispersive media using FDTD," *IEEE Trans. Antennas Propag.*, vol. 44, pp. 792–797, 1996.
[37] J. P. Bérenger, "A perfectly matched layer for the absorption of electromagnetic waves," *J. Comput. Phys.*, vol. 114, pp. 185–200, 1994.
[38] S. D. Gedney, "An anisotropic PML absorbing media for the FDTD simulation of fields in lossy and dispersive media," *Electromagn.*, vol. 16, pp. 399–415, 1996.
[39] A. P. Zhao, J. Juntunen, and A. V. Raisanen, "Generalized material-independent PML absorbers for the FDTD simulation of electromagnetic waves in arbitrary anisotropic dielectric and magnetic media," *IEEE Microwave Guided Wave Lett.*, vol. 8, pp. 52–54, 1998.
[40] W. Hu and S. A. Cummer, "The nearly perfectly matched layer is a perfectly matched layer," *IEEE Antennas Wireless Propag. Lett.*, pp. 137–140, 2004.
[41] K. G. Budden, *The Propagation of Radio Waves*. Cambridge, U.K.: Cambridge Univ. Press, 1985.
[42] H. G. Booker and W. Walkinshaw, "The mode theory of tropospheric refraction and its relation to wave-guides and diffraction," in *Report: Meteorological Factors in Radio Wave Propagation*. London, U.K.: Physical Society, 1946, pp. 80–127.
[43] J. H. Richter, "Application of conformal mapping to earth flattening procedures," *Radio Sci.*, vol. 1, no. 2, pp. 1435–1438, 1966.
[44] J. E. Bickel, J. A. Ferguson, and G. V. Stanley, "Experimental observation of magnetic field effects on VLF propagation at night," *Radio Sci.*, vol. 5, pp. 19–25, 1970.
[45] N. R. Thomson, "Experimental daytime VLF ionospheric parameters," *J. Atoms. Terr. Phys.*, vol. 55, pp. 173–184, 1993.
[46] R. Barr, "The effect of sporadic-E on the nocturnal propagation of ELF radio waves," *J. Atmos. Terr. Phys.*, vol. 39, pp. 1379–1387, 1977.

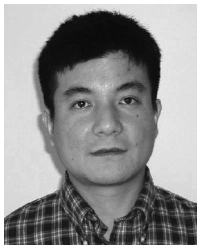

Wenyi Hu received the B.S. degree from the China Institute of Metrology, China, in 1994, the M.S. degree from Huazhong University of Science and Technology, China, in 1998, and the Ph.D. degree in electrical engineering from Duke University, Durham, NC, in 2005.

Since 2000, he has studied and worked at the Radio Remote Sensing Lab at Duke University. Currently, he is working as a Postdoctoral Research Scientist at Schlumberger-Doll Research, Ridgefield, CT. His current research interests include computational electromagnetics, lightning-upper atmosphere interactions, ionospheric remote sensing, and inverse problems.

Steven A. Cummer (M'97–SM'02) received the Ph.D. degree in electrical engineering from Stanford University, Stanford, CA, in 1997.

Previously, he spent two years at NASA Goddard Space Flight Center as an NRC Postdoctoral Research Associate. He is currently an Assistant Professor of electrical and computer engineering at Duke University, Durham, NC. He has written or coauthored more than 45 papers in refereed journals. His current work is in a variety of theoretical and experimental electromagnetic problems related to geophysical remote sensing and engineered electromagnetic materials. He has developed and implemented novel techniques for upper atmospheric remote sensing using natural electromagnetic sources, lightning remote sensing, and space plasma tomography using multisatellite radio propagation measurements.

Dr. Cummer received a National Science Foundation CAREER Award and a Presidential Early Career Award for Scientists and Engineers (PECASE) in 2001.